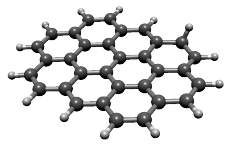

I

INTRODUCTION

"Lo que se abre ante nuestros ojos es el mundo anterior al hombre. Abajo, en los grandes ríos, quedaron los saurios monstruosos, las anacondas, los peces con tetas, los laulaus cabezones, los escualos de agua dulce, los gimnotos y lepidosirenas que todavía cargan con su estampa de animales prehistóricos, legado de las dragonadas del Terciario. Aquí, aunque algo huya bajo los helechos arborescentes, aunque la abeja trabaje en las cavernas, nada parece saber de seres vivientes. Acaban de apartarse las aguas, aparecida es la Seca, hecha es la yerba verde, y, por primera vez, se prueban las lumbreras que habrán de señorear en el día y en la noche. Estamos en el mundo del Génesis al fin del Cuarto Día de la Creación. Si retrocediéramos un poco más, llegaríamos adonde comenzara la terrible soledad del Creador — la tristeza sideral de los tiempos sin incienso y sin alabanzas, cuando la tierra era desordenada y vacía y las tinieblas estaban sobre la faz del abismo."

— ALEJO CARPENTIER, Los pasos perdidos.

Not a hundred years have passed since the discovery of the very first interstellar molecule — methylidyne (CH; Swings & Rosenfeld 1937) — and, to date, more than 200 different molecules have been detected, either in the gas phase, or as ices around dust grains.[1] Of these, polycyclic aromatic hydrocarbons (PAHs) are among the largest, most stable species detected thus far (Tielens 2008). PAHs are a family of molecules characterized by a graphene-like skeleton of carbon atoms with hydrogens terminating the edge of the molecules. They are identified through their common mid-infrared (mid-IR) emission features that are seen towards most lines of sight, but are specially prominent in regions with strong ultraviolet (UV) fields. This is aided by their high stability, as they can survive better than other species when subjected to harsh radiation.

The interest in interstellar molecules is not only limited to the chemical reactions involved in their formation and destruction, but is also related to astrophysics in general. Line emission/absorption and certain chemical processes are related to the physical conditions of the environment. As such, the molecular inventory acts as a tracer of temperatures, densities and other physical parameters that would be otherwise hard to probe.

The vast majority of the molecular species detected in space contain carbon and hydrogen atoms, signifying the important role of organic chemistry in understanding the molecular diversity of the universe. From simple chains, up to the largest observed carbon cage-like molecules, these species play a determinant role as the base for the chemistry and biology that eventually takes place on planetary systems (Herbst & van Dishoeck 2009, and references therein). The chemical pathways available in the interstellar medium (ISM) that can lead to the formation of these molecules are radically different from those commonly found on Earth. Under typical interstellar conditions of extremely low densities and temperatures, and a near constant bombardment of high energy photons, the survival of any type of chemical compounds must be accounted for when trying to understand the initial chemical makeup of newly formed planets.

For most complex molecules, direct formation via atomic or molecular reactions in the gas phase of the ISM has been proven to be highly inefficient and, as a consequence of this, alternative pathways have been proposed and investigated (Berné & Tielens 2012). The formation mechanism most commonly considered relies on reactions taking place in the ice mantles of interstellar dust grains. Such ices act as a reservoir of molecules as well as a third body capable of absorbing the excess formation energy, effectively catalyzing surface reactions even at low temperatures (Tielens 2013, and references therein). Indeed, a combination of experiments and modeling of ice mediated formation routes has led to successfully explaining the abundance of a multitude of molecules. Nevertheless, there remains the question of the chemical evolution in regions where a higher temperature and UV-field would quench to the formation of the same ice mantles. In such environments, "bottom-up" formation schemes — merging small species to create larger ones — are less effective. All this, combined with trends that speak of active formation of molecules within environments extremely hostile to this pathway, beg for the search of different types of reactions.

The detection of fullerenes and small hydrocarbons within photodissociation regions

[1] http://www.astro.uni-koeln.de/cdms/molecules

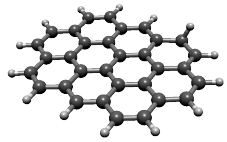

(PDRs; Sellgren et al. 2010; Boersma et al. 2012), supports the case for a formation pathway involving the photodestruction of larger precursor species. The mid-IR bands of fullerenes in particular, show a clear increase in intensity as the radiation field of the PDR becomes harsher. This is coupled with a decrease of other mid-IR bands associated with PAHs, which have been postulated as a starting point in the origin of fullerenes in PDRs (Berné & Tielens 2012). The connection of PAHs and fullerenes has led to the suggestion of an alternative formation route in the ISM, involving unimolecular photodissociation of fairly stable species (such as large PAHs). This "top-down" interstellar chemistry can give rise to fullerenes, PAH derivatives — such as dehydrogenated species or hydrocarbon chains — and can even contribute to the formation of H_2. Given that both the bottom-up and top-down processing mechanisms can occur at different evolutionary stages or, to an extent, in tandem, it must be stressed here that they should not be considered as independent and separated processes. For instance, the small hydrocarbon products of PAH dissociation can, after drifting to a different interstellar environment, be incorporated in ice mantles and act as previously unavailable precursors for a new generation of molecules (Tielens 2013).

In order to study these processes, astronomical observations cannot be used as a single, isolated tool. A variety of laboratory techniques have been proven successful in investigating a variety of solid state and gas phase reactions, providing critical parameters that can be compared to observational data (Wiesenfeld et al. 2018). These parameters include reaction rates, spectroscopic information and the characterization of the involved reaction networks. In addition, these experiments can also shed light into processes not previously considered, which have historically helped in reconciling apparent contradictions between model predictions and observations. The development of the field of experimental astrochemistry has been crucial for such advances. While the contributions from chemistry into astronomy cannot be overstated, the characterization of molecules and compounds under the exotic conditions of the ISM are not an obvious avenue of research within that field. The continued advancement within astrochemistry not only allow for the interpretation of astronomical data, but also sheds light into the working of chemical reactions that are simply not available within an earthbound context.

Much progress has been made in mimicking the conditions of a variety of interstellar environments but, even under the most favorable of circumstances, they only provide an approximation to the actual physical conditions encountered within the ISM. In particular, the timescales involved in most astronomical processes are completely beyond the realm of experimental feasibility. It is in bridging these gaps that modeling tools become not only relevant, but absolutely essential for understanding the large scale impact of molecular processing. Furthermore, quantum chemical calculations have continuously helped in understanding the molecular characteristics that contribute to the reactions observed within experimental works and in predicting how similar molecules will behave in a manner that is more time efficient than rigorous experiments. This is not to say that continued experiments are no longer required, given that the validity of the trends derived in this manner needs to be carefully scrutinized and corroborated (Wiesenfeld et al. 2018).

The overall goal of this thesis is to gain new experimental, theoretical and observa-

tional knowledge of the photofragmentation of PAHs and their relation to interstellar top-down chemistry. The focus will be on the identification of stable photoproducts and the characterization of the main reactions leading to them. In particular, we will explore the formation of both fullerenes and molecular hydrogen. A chemical connection between PAHs and fullerenes has indeed been suggested before, but further exploration of this hypothesis, together with experimental evidence for this process, is presented here. The production of H_2 in dense PDRs has proven to be an elusive question, with observational estimates of the formation rate differing by as much as an order of magnitude with respect to the processes taken into account (Habart et al. 2004). The first step in the photofragmentation of PAHs involves their dehydrogenation, with one of its possible pathways including the release of an H_2 molecule as part of the process (Ling et al. 1995; Zhen et al. 2014). We study here the significance of this fragmentation channel and present its relevance for molecular hydrogen production in the ISM.

This introduction will expand on the topics touched upon thus far, detailing the astronomical context and main questions regarding the interstellar organic inventory in general and PAHs in particular. A brief historical overview on the development of the PAH hypothesis and related species will be provided as well, together with future research prospects involving the next generation of space telescopes. We will also discuss the variations observed in the mid-IR spectra of interstellar PAHs and how they have been related to subfamilies within the broader category of aromatic molecules. Theoretical and experimental results related to trends within PAHs will follow, as well as a discussion of their excitation/deexcitation mechanisms and the fragmentation pathways that have been characterized up to this point. Finally, we will delve into the top-down formation route, linking together the information thus far presented within this introduction as a launching pad for the main topics discussed within this thesis.

1.1. Astrochemistry and organic inventory

Figure 1.1 shows a non-exhaustive sample of the molecules that have been detected in the ISM, as well as how the number of identifications has evolved over time. From the first detections at the end of the 30's, there were barely any new molecules reported until the 70's, when the rate of positive identifications exploded and with 4–5 new identifications per year has remained nearly constant since then. The first generation of molecules observed (CH, CH^+) were detected through their absorption in the visible spectrum, although the lack in theoretical an experimental data delayed the confirmation of these detections (McKellar 1940). The great increase in the total number of molecules identified from the 70's onwards relied mostly on the refinement of radioastronomy, as well as on an extended catalog of molecular rotational transitions, thus allowing for the detection of the first true polyatomic molecule, formaldehyde (H_2CO; Zuckerman et al. 1970). These early identifications were dependent on the observation of rotational transitions, which are found at millimeter/submillimeter wavelengths. However, this is not the only spectral range within which molecular transitions can be found. The infrared hosts a variety of vibrational and rovibrational transitions of different molecules, although vibrational bands are more sensitive to the nature of spe-

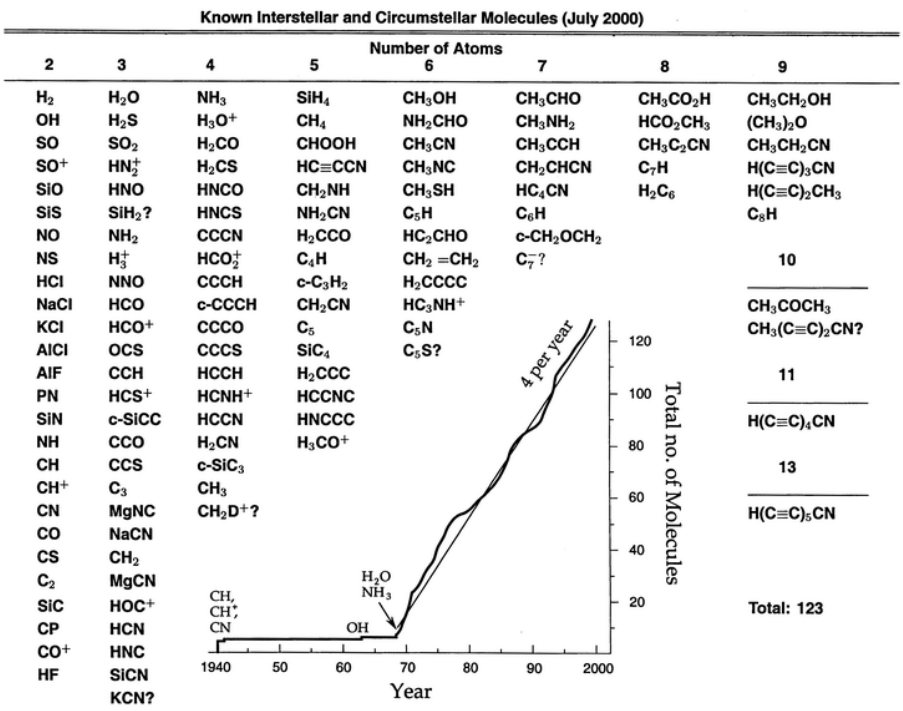

Figure 1.1.: List of molecules detected in interstellar and circumstellar material up to the year 2000, organized by the number of atoms in the molecule in question. Note that all molecules with six or more atoms contain at least one carbon in their structure. The inset shows the evolution in the number of molecules discovered as a function of year (Figure taken from Thaddeus & McCarthy 2001).

cific bonds within the molecule rather than the full molecular structure (Badger 1934). The development of infrared astronomy has progressed more slowly, due to the atmosphere being opaque to a large part of this range of the electromagnetic spectrum and thus generally requiring observations from space or with very high altitude telescopes.

The molecules identified thus far in the ISM reveal a large range of chemical reactions and atoms involved in the molecular complexity of the universe. Nevertheless, a clear trend is apparent from Fig. 1.1; carbon bearing molecules dominate the overall population of detected species, particularly towards larger masses. No molecule with six or more atoms lacking carbon has up to date been identified, making organic chemistry a prominent field within astrochemistry. This is not due to any particular kind of bias in the detected molecules, but it is to be expected due to interstellar abundances and the atomic properties of carbon. Being the fourth most abundant element in the universe — behind hydrogen, helium and oxygen — the ubiquitousness of organic molecules is no surprise. Further cementing the preponderance of carbon bearing molecules is the possibility for carbon to create large complex molecules and bond in a

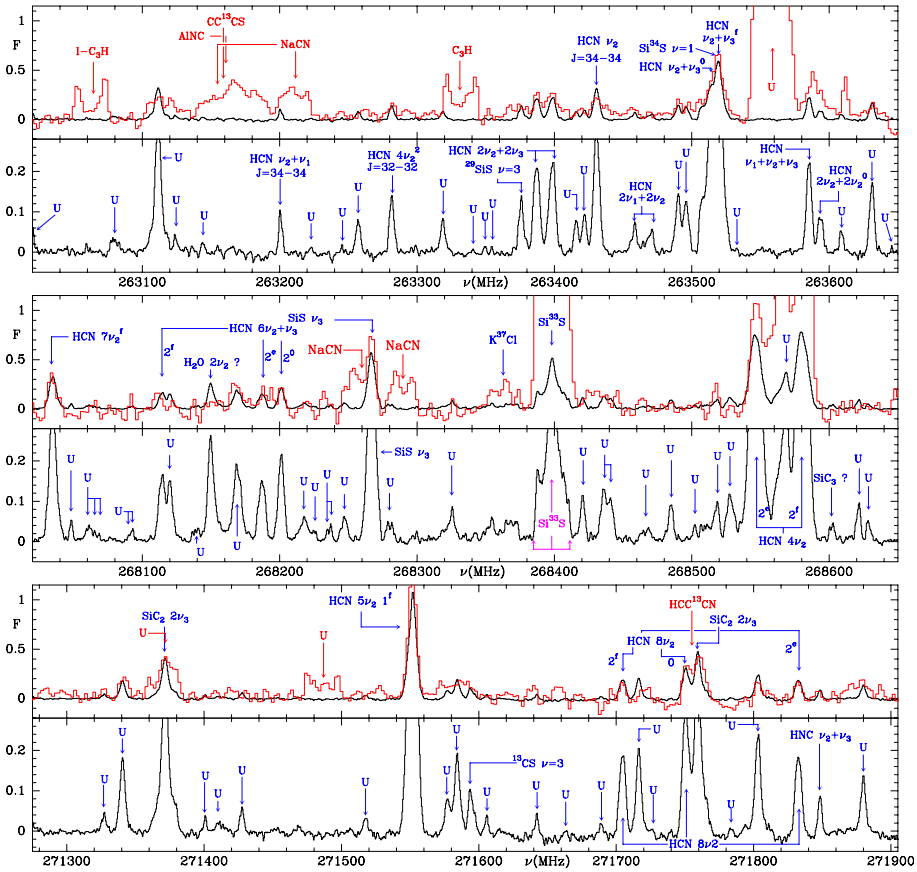

Figure 1.2.: Comparison of ALMA (black) and 30-m IRAM spectra (red) of IRC+10216. The intensity scale is in units of Jy beam^{-1}. The bottom panel shows a zoom-in of the ALMA observations. Molecular transitions labeled in red were detected with the single dish of IRAM, but filtered out by the ALMA interferometer. Lines labeled U correspond to emission lines as of yet unidentified (Figure taken from Cernicharo et al. 2013).

variety of forms. This very same property has made organic chemistry so determinant for the formation and evolution of complex life here on Earth. In recent years, a wide arrange of complex organic molecules have been detected in space, including a sugar (glycolaldehyde, $HOCH_2CHO$; Jørgensen et al. 2012), a simple amino-acid (glycine, NH_2CH_2COOH; Kuan et al. 2003) — although this detection remains somewhat uncertain (Snyder et al. 2005) — and an example of a chiral molecule (1,2-propylene oxide, CH_3CHCH_2O; McGuire et al. 2016). With the advent of the ALMA interferometer, a veritable forest of weak unidentified transitions has been detected (Fig. 1.2), suggesting that further detections might be ahead.

The variety of the bonding characters available for carbon relates to the formation of hybrid orbitals, which involve the mixing of individual atomic orbitals that can later

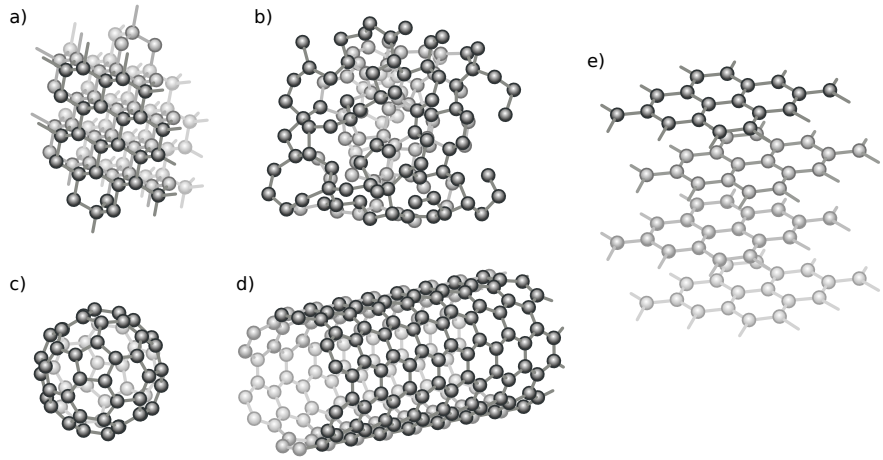

Figure 1.3.: Different allotropic forms of pure carbon materials. a) Crystalline structure of diamond, showcasing a pure sp^3 hybridization. b) Amorphous carbon can display a mixture of the three possible hybridizations, with the exact ratios depending on the particular structure. c) Buckminsterfullerene (C_{60}); the fullerene family displays sp^2 hybridization. d) Carbon nanotubes can be seen as a one-dimensional extension of fullerenes, and as such are also an example of sp^2 hybridization. e) Graphite consists on weakly bounded graphene (sp^2) sheets, which are representative of the structure of PAHs (Figure by J. Sivek/CC BY-SA 4.0).

pair electrons to form covalent bonds, with the character of the bond established by the type of hybridization involved. Carbon can be found in a variety of hybridization types, mixing a number of $2s$ and $2p$ orbitals, which in turn lead to diverse geometrical arrangements of bond structures. These hybridized orbitals include sp^3, sp^2 and sp, which allow for the formation of four, three and two σ bonds, respectively. The remaining electrons in unhybridized atomic orbitals in the case of sp^2 and sp hybridization can be used for one or two additional π bonds, respectively. Figure 1.3 displays different allotropic forms of carbonaceous materials together with their respective hybridization. Of these, fullerenes have been conclusively detected in the ISM (Cami et al. 2010), along with diamondoids (Guillois et al. 1999) and PAHs (Allamandola et al. 1985), the hydrogenated molecular forms of diamond and graphene, respectively. The different hybridizations of carbon are also represented among the simpler carbon bearing molecules detected in the ISM. For instance, methane (CH_4) has four σ bonds and is thus both sp^3 hybridized and fully saturated, while acetylene (C_2H_2) has sp hybridization and the triple bond between the carbon atoms consists of one σ and two π bonds. Carbon molecules with double bonds are representative of sp^2 hybridized orbitals.

The case of interstellar PAHs is of particular interest for the organic inventory of the ISM. A standard PAH molecule has a honeycomb-like structure of linked hexagonal carbon rings terminated in hydrogen atoms, examples of which are presented in Fig. 1.4. This results in thousands of possible geometries, varying in size and compactness. While the identification of a specific PAH has remained elusive — barring

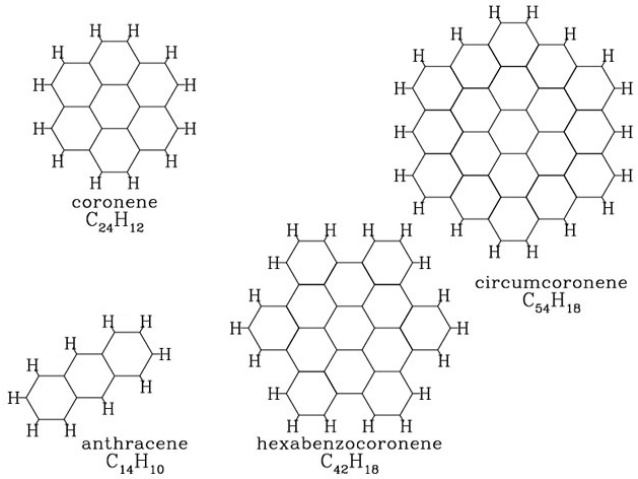

Figure 1.4.: Example of PAH molecules spanning a large range in sizes, from three fused rings (anthracene) to nineteen (circumcoronene). The hexagonal carbon rings are characteristic of standard PAHs, but modified structures with five and/or seven membered rings can also be found (Figure adapted from Draine 2010).

a tentative detection through blue fluorescence of anthracene and pyrene in the Red Rectangle (Vijh et al. 2004) —, the mid-IR spectra of most galactic objects and several extragalactic sources betrays their ubiquitous presence (Tielens 2008). The spectral characteristics of PAHs will be discussed in detail later on (Sect. 1.5.1), but suffice it to say here that their mid-IR bands are characteristic of specific atomic bonds rather than of particular molecules. PAHs are among the largest molecules found in the ISM, containing about 50–100 C-atoms each and observational evidence suggests that they lock up to 10–20% of all elemental carbon (Allamandola et al. 1989). Besides their near universal presence in the ISM, laboratory studies indicate that they can form more complex organic molecules through hydrogenation, oxygenation and hydroxylation when locked up in ices, paving the way towards amino-acids and other biological molecules (Gudipati & Yang 2012). PAH evolution in the gas phase has also sparked considerable interest, as they are postulated to be a starting point for top-down interstellar chemistry (Berné & Tielens 2012), as their fragmentation can give rise to a variety of molecules not accessible through solid state reactions (a more in-depth view into this mechanism will be provided in Sect. 1.4).

PAHs are not only relevant for astronomy on the grounds of their involvement in the chemistry of the ISM, but also because they can act as tracers for the physical conditions of the variety of regions where they are found. PAHs, specially as their size increases, have relatively low ionization potentials, making them a primary source of electrons in PDRs, where most of the atomic gas is neutral. This, coupled with their efficient recombination with electrons, in turn sets the ionization balance of the neutral medium of the galaxy. The ionization of PAHs is also determinant in controlling the

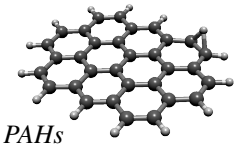

energy balance of HI regions, via the photoelectric effect, which is known to be the dominant heating mechanism in these regions (Hollenbach & Tielens 1999). While the photoelectric effect from prototypical dust grains also takes part in heating the neutral medium, the heating efficiency is dominated by the lower end of the size distribution, which is thought to overlap with that of the largest PAHs.

The mid-IR emission bands from PAHs are also used to trace the hardness of the UV-field. These bands are emitted by vibrationally excited PAHs cascading down to their ground state following the absorption of an energetic far-UV photon originating from the interstellar radiation field. The absorbed photon will directly lead to an excited electronic state, the energy is then transferred into the vibrational modes via internal conversion and intramolecular vibrational redistribution in a short timescale of $\sim 10^{-9}$ s (Allamandola et al. 1989). This connection between PAH emission and the intensity of the UV-field has proven particularly useful for tracing star forming regions in high redshift galaxies (Genzel et al. 1998). Signs of PAH emission can help distinguish between excitation due to active galactic nuclei (AGNs) and that due to massive stellar formation (Pope et al. 2007). Thus far this technique has allowed for the identification of star forming galaxies up to $z \sim 3$, but the imminent launch of the *James Webb Space Telescope* (*JWST*) is expected to push this limit much farther back.

As remarkable as the progress of the last fifty or so years has been, several lingering questions remain within astrochemistry in general, and PAHs in particular. Laboratory evidence suggests that the formation of biomolecules such as amino-acids is indeed feasible under interstellar conditions, observational confirmation on the presence of such species is still lacking (Nuevo et al. 2014). There is as well the issue of up to what extent molecular complexity can develop in the ISM prior to planet formation and, perhaps more importantly, which species can survive and effectively be delivered to newly formed planets along the evolutionary stages of collapsing dense clouds, proto-planetary disks and the formation of young stellar objects and new planetary systems (Kwok 2016, and references therein). PAHs are a crucial piece of this puzzle given their widespread presence in the ISM and the significant amount of carbon locked up in them. The processing of PAHs under UV radiation holds the potential to open up previously unconsidered chemical pathways and may deliver the precursors of biologically significant species (Tielens 2013). The studies presented in this thesis focus on such processing, in order to examine which products are the most stable ones, to study the details of the reactions that can produce them and what is their impact on interstellar chemistry.

1.2. Historical overview on interstellar PAHs

While the origin of IR astronomy can be traced back all the way to the 19th century, its development in earnest had to wait until the 1960's and 1970's (Rieke 2009). A fundamental step in this direction came with the use of airborne telescopes, such as the Kuiper Airborne Observatory (KAO Cameron 1976), and later with space based telescopes, such as the *Infrared Astronomical Satellite* (*IRAS*; Neugebauer et al. 1984). Spectroscopic observations with ground based telescopes and KAO showed from early

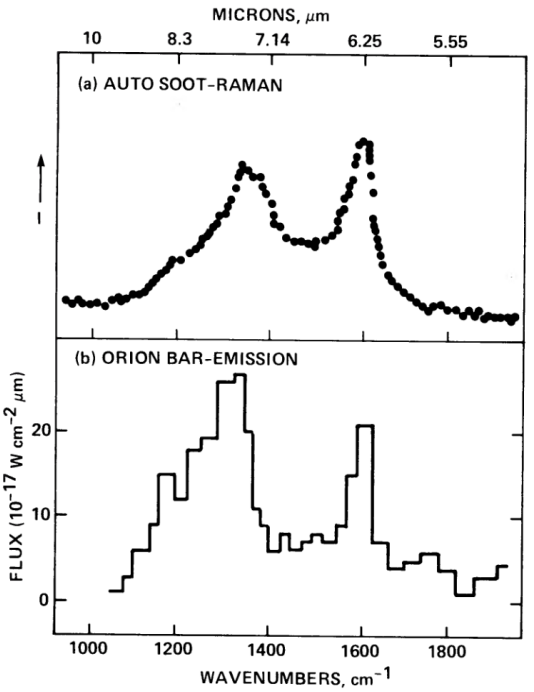

Figure 1.5.: Comparison of an experimental Raman spectrum of soot from a car exhaust, which is dominated by emission of PAHs (Rosen & Novakov 1978) (a), and astronomical observations of the Orion bar reflection nebula (b) in the 5 to 10 μm spectral range (Bregman et al. 1983) (Figure taken from Allamandola et al. 1985).

on a series of previously unknown emission bands, with the strongest found at 3.3, 6.2, 7.7, 8.6 and 11.2 μm (Gillett et al. 1973; Russell et al. 1977). These emission bands were dubbed the unidentified infrared bands (UIB). Additionally, an excess emission was detected with *IRAS*, most prominently in the band at 12 μm (Aumann et al. 1984). This mid-IR excess could not be explained by dust in radiative equilibrium alone, since this could only be explained with unrealistically high dust grain temperatures. A population of very small grains (VSGs) where proposed to account for the observation, given that the low heat capacity would transiently excite these molecules to high temperatures. As such, this grain population would not be in radiative equilibrium, but rather be stochastically heated (Sellgren 1984; Léger & Puget 1984). The VSG hypothesis required a range in grain sizes corresponding to a few hundred atoms, which could more properly be considered large molecules

The presence of aromatic molecules in the ISM had already been proposed in the form of the carriers of the UV extinction bump at 2175 Å (Draine & Lee 1984). However, the interest in this family of molecules was renewed with the realization that they fulfilled the main tenants of the VSG hypothesis (Léger & Puget 1984). A crucial step forward in identifying PAHs as the carriers of the UIBs came from the comparison of

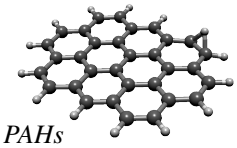

astronomical spectra to laboratory experiments on soot from car exhaust, as shown in Fig. 1.5 (Allamandola et al. 1985). The exhaust gases consist of a mixture of PAHs and other graphitic material, which are known to be the result of incomplete combustion (Rosen & Novakov 1978). This positive identification helped bringing along collaborations with experimentalist and theoretical chemists. The combined efforts of these disciplines have resulted in a vast spectroscopic database of different PAHs and related species, all of which support the connection between the mid-IR bands and PAHs (e.g., Boersma et al. 2014; Hudgins & Sandford 1998; Oomens et al. 2006). As the evidence mounted, and the PAH hypothesis started gathering widespread acceptance, the UIBs came to be known as the aromatic infrared bands (AIB). It must be noted though, that a fair share of criticism has also been leveled at the hypothesis, with carriers such as hydrogenated amorphous carbon (HAC) being proposed as an alternative (Zhang & Kwok 2015).

Analogous to the known formation mechanism of PAHs in soot, a formation route was proposed in the shell of asymptotic giant branch (AGB) and post-AGB stars (Frenklach & Feigelson 1989; Cherchneff et al. 1992). The formation of interstellar dust in general has also been associated with these latter stages in stellar evolution, and whether the formation leads to carbonaceous or silicate based grains will depend on the C:O ratio in the envelope of these dying stars. Experiments aimed at understanding the relevance of this formation mechanism were key in identifying a new allotrope of carbon: fullerenes (Kroto et al. 1985). The prototypical icosahedral C_{60} fullerene had actually been proposed as a new molecular form of carbon in the 1970's, but it failed to gain traction in those days (see Thrower 1999, for a historical overview). It was later noticed that fullerene formation in soot-like environments was not only confined to laboratory conditions and was a much more general process (Krätschmer et al. 1990). Twenty-five years had yet to pass from the finding of fullerenes to their detection in the ISM (Fig. 1.6a; Cami et al. 2010; Sellgren et al. 2010). As was the case for PAHs, their mid-IR bands were determinant in identifying their presence in planetary nebulae (PNe) and PDRs.

Once the ubiquitousness of PAHs in the ISM had been well established, the search for evidence of electronic and rotational transitions started as well. One avenue of research was the attempt at identifying PAH signatures among the diffuse interstellar bands (DIBs) which are observed in absorption towards most stars within the galaxy (Snow 2001). DIBs have been recognized and classified since the interwar years (Heger 1922), and it has been well established that they are interstellar in origin (Merrill et al. 1937; Merrill & Sanford 1938). Electronic transitions of neutral PAHs typically fall at wavelengths shorter than those of most DIBs, but PAH cations have their main absorptions further to the red. For this reason, research connecting the DIBs and PAHs has been mostly limited to charged species (Snow et al. 1998). However, a positive match of one or more DIBs to any particular PAH has proven elusive to this day. More success has recently been found in terms of identifying fullerenes as carriers of some of the DIBs. Although C_{60}^{+} was proposed as the source of two near-IR DIBs (at 9577 and 9632 Å; Foing & Ehrenfreund 1994), this first assignment was based on the results of matrix spectroscopy and thus the identification was not deemed conclusive (Maier 1994). It would not be until Campbell et al. (2015) measured the gas-phase absorption

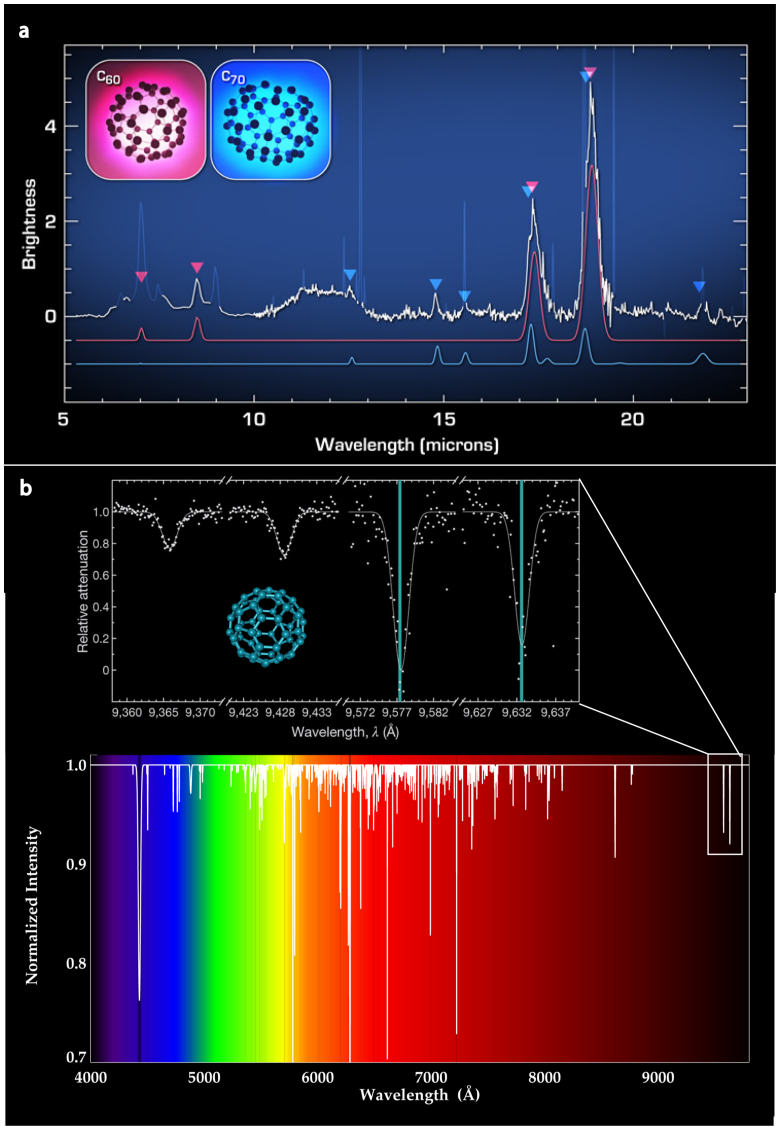

Figure 1.6.: Observational evidence for the presence of fullerenes in the ISM. a) *Spitzer* mid-IR spectrum of the planetary nebula Tc 1 (white), compared with theoretical spectra of the C_{60} (red) and C_{70} (blue) fullerenes (Cami et al. 2010). b) Near-UV to near-IR spectrum showcasing the main known DIB absorption bands. The inset presents the experimental gas-phase spectra of C_{60}^{+} with the two vertical lines highlighting the position of the DIBs first associated to these absorptions (Campbell et al. 2015). The two other experimental bands also seem to have DIB counterparts. Image credits for DIB spectrum: J. Cami; for Tc 1 spectrum: NASA/JPL-Caltech/J. Cami (Figure provided by A. Candian).

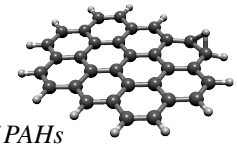

of helium tagged C_{60}^+ in a cryogenic ion trap that stronger evidence on the origin of these bands was provided (Fig. 1.6b).

The search for pure rotational transitions of PAHs presents a different type of challenge. Traditional PAHs lack a permanent dipole moment, because of their high symmetry, thus making such transitions forbidden. Nevertheless, an interest on the rotational spectroscopy of these molecules arouse out of the detection of a previously undiscovered galactic foreground in observations aimed at mapping the cosmic microwave background (Leitch et al. 1997). This foreground, dubbed anomalous microwave emission (AME), peaks at around centimeter wavelengths and it has been theorized to arise from rapidly rotating VSGs (Draine & Li 2001). As was the case in the identification of the AIBs, these VSGs straddle the line between large molecules and bulk materials, and the possible contribution of PAHs to the AME has been considered from the beginning. In order to circumvent the lack of permanent dipole moment, research has focused on modified PAHs, whether through the addition of subgroups, partial fragmentation or non-planar (bowl-shaped) PAHs (Pilleri et al. 2009). As with the DIBs, an incontrovertible identification of PAHs through AME has not been possible thus far.

Although research on interstellar PAHs has not been limited to mid-IR spectroscopy, it is indubitable that this has been the most successful technique and a large part of future work on this topic remains tied to it. From the first detections of the AIBs with the instruments of KAO, advances in technology and multinational collaborations have done much in order to advance the field. The first orbital telescope with spectroscopic capability in the mid-IR was the *Infrared Space Observatory* (*ISO*; Kessler et al. 1996). It helped cementing the bases of the PAH hypothesis and its higher spectral resolution allowed for the creation of a classification of AIB spectra, based on variations in band intensities and shapes. The next generation IR orbiting observatory came with the *Spitzer Space Telescope* (Werner et al. 2004), which added the capability of creating spectral maps. This tool allowed for the first time to observe AIB spectral variations within a single source, and was indispensable in establishing the relationship between the photodestruction of PAHs and the formation of fullerenes in PDRs. The imminent launch of *JWST* promises to extend on this capabilities with its improved spectral and spatial resolution.

1.3. Observational characterization of PAHs

As mentioned in the previous section, observational studies have been a driving force behind our current understanding of the evolution of PAHs in space. Their resilience against photofragmentation allows for these molecules to survive for longer periods of time in a wide variety of interstellar and circumstellar environments, whereas other species are easily fragmented and revert to their atomic components when outside highly UV-shielded regions. Their mid-IR signatures have been detected in the diffuse ISM, PNe, post-AGB stars, star forming regions and protoplanetary disks, both within our galaxy and in extragalactic sources (e.g. Fig. 1.7; see Tielens 2008, and references therein). The driving physical mechanism behind IR fluorescence requires

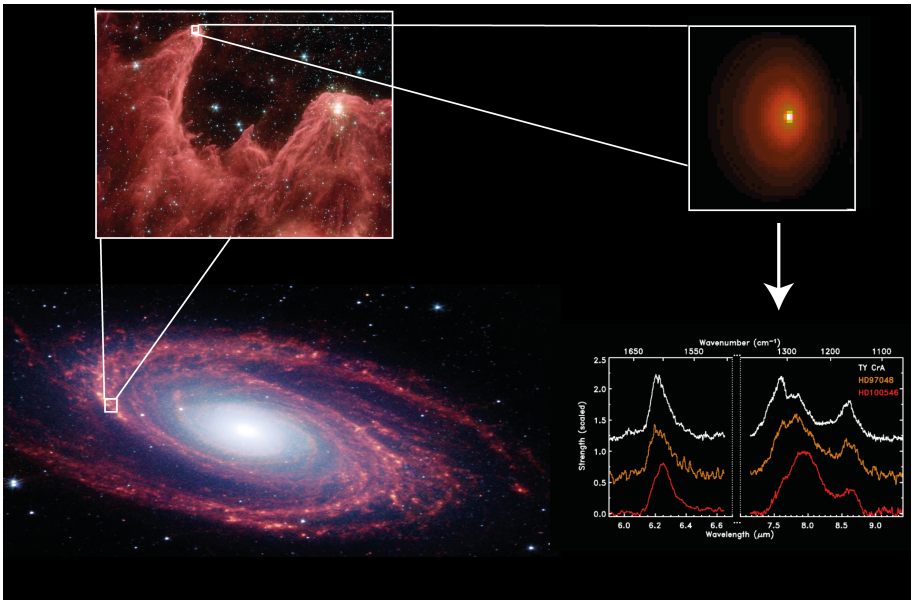

Figure 1.7.: PAHs dominate the mid-IR emission in the universe. Lower-left: Composite image of M 81 as taken by *Spitzer*. Red corresponds to emission at 8.0 μm, which is dominated by PAHs. Upper-left: The Mountains of Creation in the Soul Nebula (IC 1871), with red again associated with the 8.0 μm filter of *Spitzer*. Top-right: Protoplanetary disk around HD 97048 observed with the 8.6 μm filter of the Very Large Telescope (VLT; image adapted from Doucet et al. 2007). Lower-right: PAH spectra of three different protoplanetary disks (image adapted from Boersma et al. 2008). Image credits for M 81, Mountains of Creations: NASA/JPL-Caltech/Harvard-Smithsonian CfA (Figure provided by A. Candian).

the presence of strong UV-fields for the AIBs to be observed. In addition to this, it is expected that in well shielded environments PAHs will coagulate or be incorporated into the ice mantles of dust grains. This thesis focuses on the chemical evolution of PAHs within PDRs associated with star forming regions, which begs for a description of the physical and chemical conditions most commonly found in these regions.

1.3.1. Photodissociation regions

PDRs can be briefly described as mostly neutral regions in the ISM where intense UV-fields dominate the energy balance and chemical conditions of the gas (Hollenbach & Tielens 1997, 1999). It is within these environments that a transition from largely atomic to largely molecular gas takes place. Their structure follows a layered pattern as the gas temperature, $T_{\rm gas}$, decreases, beginning from the transitional area where protons and electrons recombine into hydrogen atoms (Fig. 1.8). The first molecule to be formed is H_2, for which the transition occurs at $A_V \simeq 2$. This zone also corresponds to the peak of PAH emission, where they are found to be mostly ionized owing to their

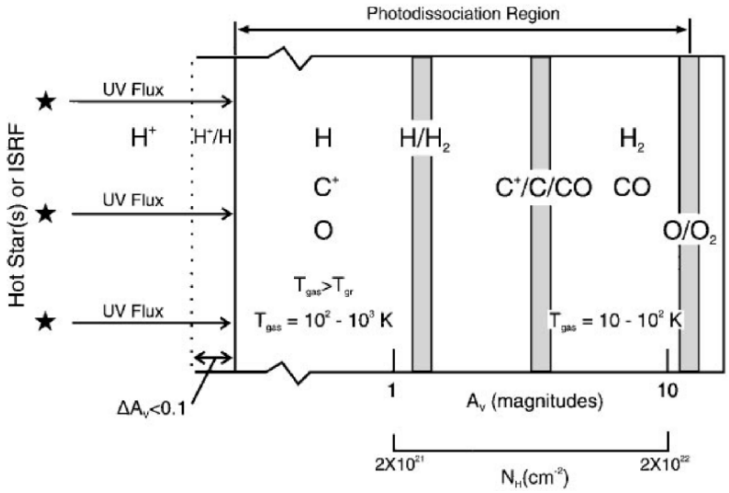

Figure 1.8.: Diagram of the typical structure of PDRs, with the HII dominated region to the left and the molecular cloud on the rights. The main atomic to molecular transition regions are sketched above, together with typical gas temperatures and column densities (Figure taken from Hollenbach & Tielens 1997).

low ionization potential (typically from 6 to 10 eV). Carbon atoms also remain ionized deeper into the PDR, up to $A_V \simeq 4$, at which point they will be able to recombine and quickly react with atomic oxygen to form CO, the second most abundant interstellar molecule. The edge of the PDR on the molecular cloud side is roughly defined by the area in which the remaining oxygen can be turned into O_2, at which point almost all the gas is in molecular form.

The aforementioned structure of the PDR is determined by the number density of the region in question, n, and the intensity of the incident UV-field expressed in units of the average UV interstellar radiation field (Habing 1968) — i.e., $G_0 = 1$ equals 1.6×10^{-3} erg cm^{-2} s^{-1}. Under these circumstances it is clear that the parameter G_0/n will dominate most processes within the PDR, including the ionization balance. While the term PDR is generally used to refer to the dense medium surrounding star forming regions, in reality it encompasses most of the diffuse ISM, as well as the circumstellar material irradiated by the remnants of evolved stars. The flared sections of protoplanetary disks can also be considered PDRs on their own right, as the cold molecular gas and dust in the mid-plane transition towards regions where simple molecules formed in ices can be evaporated and subsequently photodissociated.

The far-UV fields dominate most processes within PDRs but, considering the outlined structure of these regions, there are limits to the photon energies available. Photons with energies above 13.6 eV — the ionization potential (IP) of atomic hydrogen — can exclusively be found in HII regions bordering PDRs, and are thus not significant within. Carbon can remain ionized throughout a large portion of the PDR, owing to its IP being 11.3 eV, and the same is true for most PAHs. Molecular hydrogen has a

bond dissociation energy of 4.3 eV, but the H/H_2 transition happens much earlier than carbon recombination. The first electronically excited state of H_2 is unbound, but due to it being a triplet state makes the transition from the singlet ground state forbidden. As such, photodissociation goes through the absorption of a UV photon in allowed transitions (the closest one requiring 11.2 eV) followed by spontaneous emission into the vibrational continuum of the ground state (Abgrall et al. 1992). While the energy of this process is similar to that of carbon ionization, the fact that the photon absorption in the former process occurs through discrete transitions makes self-shielding efficient, as the presence of foreground H_2 molecules will use up most photons with at frequency.

PAHs are found throughout all zones in PDRs, although they are subject to different types of processes depending on their size and location. The IP of the smallest PAHs is about 7–8 eV and it decreases as the size increases. Ionization of PAHs is the most important source of gas heating within PDRs, together with photoelectric heating from dust grains (Bakes & Tielens 1994). When reaching the H_2 photodissociation front, PAH fragmentation starts to take place. As photons are absorbed and the electronic energy is transfered into the vibrational degrees of freedom, different bonds within the molecule can be severed and a series of fragments can be released. The first dissociation channels to open up involve hydrogen loss, whether atomic or molecular but, as the energy increases, carbon containing fragments can be lost as well (Jochims et al. 1994). Observations of small hydrocarbons, unaccounted for in chemical models of PDRs, suggest that they could be formed following fragmentation of PAHs (Pety et al. 2005). Additionally, the intensity of PAH bands has been observed to decrease when approaching the radiation source, while bands associated to fullerenes become more prominent (Berné & Tielens 2012).

The formation of H_2 in PDRs remain an open question. Observational constrains show a high formation rate that cannot be accounted for solely based on dust grain catalyzed reactions (Habart et al. 2004; Wakelam et al. 2017). Attempts have been made in matching the observed formation rate with reactions involving superhydrogenated PAHs, but it has been found not to be an efficient channel given the low binding energies for additional carbons (Bron et al. 2014; Andrews et al. 2016). Direct photodissociation via H_2-loss has also been considered, but so far it relies on extrapolation of dissociation parameters of small PAHs and has failed to account for the high H_2 formation rate in PDRs (Andrews et al. 2016).

1.3.2. Spectral variations of PAHs

The AIBs correspond to emission from vibrationally excited PAHs, with the main bands lying at 3.3, 6.2, 7.7, 8.6 and 11.2 μm. The band positions and their relative intensities carry information on the structure and ionization state of the emitting PAHs (Fig. 1.9). In the ISM, the only effective method to reach highly excited vibrational states is through photon absorption. However, in the case of PAHs and other organic molecules, direct photon absorption into vibrationally excited states is highly inefficient. The absorption of a UV photon creates an electronically excited molecule which then can then relax through several possible routes, such as ionization and collisional deexcitation. The former is important if the UV photon in question has an energy higher

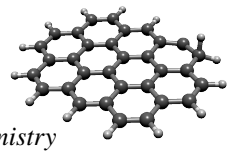

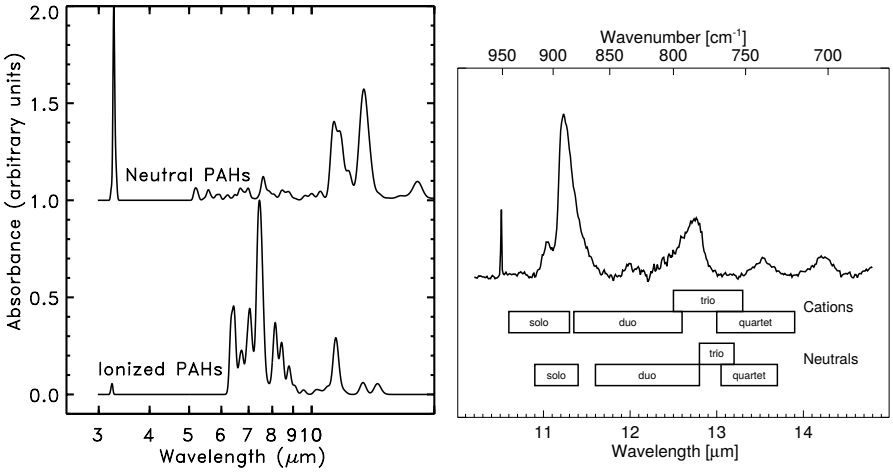

Figure 1.9.: Influence of charge and structure on the mid-IR bands of PAHs. Left: Laboratory measurements of variations in intensity due to charge. Neutral PAHs have the strongest modes in the 3 μm region (C–H in-plane modes) and 10–15 μm (C–H out-of-plane modes), while ionized PAHs are dominated by emission bands between 6 and 9 μm (C–C modes) (Figure taken from Allamandola et al. 1999). Right: Average mid-IR spectrum in the 10–15 μm region, with the band positions of C–H out-of-plane modes highlighted according to the associated edge structure (Figure taken from Hony et al. 2001).

than the IP of the particular PAH, while the latter is, as was mentioned before, usually negligible in the ISM. The PAH can rapidly ($\sim 10^{-12}$ s) undergo internal conversion (IC) into a highly vibrationally excited, lower lying electronic state. Intersystem crossing (ISC) is similar in nature to IC, but it happens at a slower rate ($\sim 10^{-9}$ s) since it involves an electronic state with a different multiplicity — e.g., from singlet to triplet states in small neutral PAHs. Both these processes are followed by intramolecular vibrational redistribution (IVR), which distributes the energy among all accessible vibrational modes in less than a nanosecond. After IVR has taken place, the relaxation process can follow through either fragmentation or IR fluorescence, which gives rise to the mid-IR band emission (Allamandola et al. 1989).

1.4. Top-down chemistry

For the most part, the formation of molecules in the ISM has focused on (ion-molecule) gas phase and solid state interactions of radicals within icy mantles surrounding dust grains. This follows a bottom-up approach, as smaller units join together to form larger compounds. This has been a fruitful research avenue, successfully reproducing observations in many cases, and providing multiple and efficient mechanisms of formation for a variety of molecules in molecular clouds, hot cores and protoplanetary disks (Herbst & van Dishoeck 2009). Furthermore, experiments aimed at reproducing

reactions in interstellar ices have pointed at the possibility of forming highly complex molecules under these conditions, although they are yet to be detected (Nuevo et al. 2014). Despite this success, there are observational trends suggesting the active formation of large, complex molecules (particularly fullerenes) in environments where the deposition of atoms and molecules on ices is not effective. Ion-molecule reactions in the gas phase would also be ineffective since they would require too many steps to build up to such complex molecules. Due to this, alternative formation routes have been postulated for these species. The most prominent of such pathways — and central focus of this thesis — involves a top-down approach, with the fragmentation of large molecules leading to different products (Berné & Tielens 2012; Berné et al. 2015).

Several observational clues have hinted at the relevance of top-down chemistry, particularly within PDRs. Many small hydrocarbon chains and cyclic structures — C_2H, C_3H_2, C_3H^+ and C_4H — have been detected towards the PDR at the edge of the Horsehead Nebula (B 33, Pety et al. 2005; Guzmán et al. 2015; Cuadrado et al. 2015). These molecules are only detected in regions of high UV photon flux and the models available failed to reproduce their presence. It was hypothesized that fragmentation of PAHs or other large, carbon bearing molecules could be responsible for the formation of these hydrocarbons. Furthermore, shortly after the discovery of fullerenes in the interstellar medium, it was realized that in NGC 7023 the fraction of carbon locked in PAHs shows a strong anticorrelation with the fraction of carbon locked in fullerenes. The increase in the population of fullerenes occurs in close proximity to the illuminating star of the PDR, again suggesting that the destruction of PAHs in particular leads to molecules whose formation in ices within these environments is highly unlikely (Berné & Tielens 2012).

The same work postulated the basis of top-down chemistry from PAHs, with the competition of fragmentation and isomerization leading to the formation of a multiple carbon and hydrocarbon molecules (Fig. 1.10). However, most of these species are highly susceptible to further dissociation, resulting in low lifetimes under interstellar conditions. For this reason, exploration into this hypothesis must by force be focused on the most stable products of PAH photofragmentation. The present formulation of top-down chemistry on the basis of fullerene observations is thus no coincidence, as these molecules are known to have high stability against dissociation. Nevertheless, other stable products can provide additional support for this type of processing. For instance, the formation of molecular hydrogen in PDRs is known to be larger than expected when considering formation on grains alone (Habart et al. 2004). Given that H_2-loss is one of the dissociation channels associated with PAH photofragmentation, a detailed look into this process might hold the key in breaching this disparity.

Finally, photon induced top-down chemistry originating in PAHs fits within the generally accepted lifecycle of PAHs in the ISM (Andrews et al. 2015; Peeters et al. 2017). Carbonaceous grains represent a significant part of interstellar dust and are thought to be formed of amorphous carbon, with a significant graphitic fraction as inferred from the 2175 Å bump in the extinction curve. Collisions and irradiation can break down the dust grains, with the aromatic, graphite-like portions able to survive for extended periods of times. This results in a wide variety of PAHs being released into the gas phase, with different sizes and structures. The PAH population will eventually become dom-

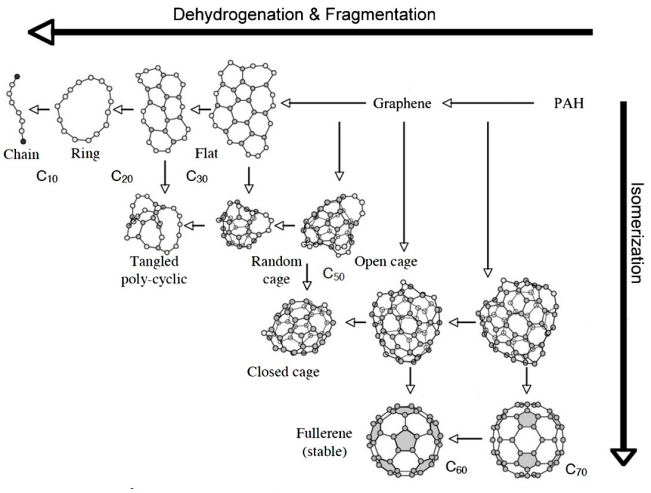

Figure 1.10.: Overview of top-down chemistry from PAHs showing possible products of PAHs through a mixture of fragmentation (right to left) and isomerization (top to bottom). Most of these fragments are themselves easily fragmented, but a few of them (such as C_{60} and C_{70}) are stable enough to endure and build up their population. This diagram does not include secondary fragments such as H_2, C_2, C_2H_2, etc. (Figure taken from Berné & Tielens 2012).

inated by a selection of large, symmetric PAHs (grandPAHs), as only the most stable among them can withstand for long under the harsh UV irradiation. Eventually, even these grandPAHs will begin to fragment, giving rise to the aforementioned top-down chemistry, with a significant fraction of them ending up locked into fullerenes.

1.5. Research methods

PAHs have a range of structural characteristics which will affect their mid-IR bands and stability against photodissociation. An important factor influencing both these aspects has to do with the symmetry of PAHs, with more symmetric compact PAHs generally being more resistant to fragmentation. Symmetry also has an effect in the mid-IR bands, given that there is a larger number of IR active modes in irregular molecules. Additionally, PAHs can be found in superhydrogenated states, have heteroatom substitutions (where a carbon is replaced by another element), five-/seven-member ring defects or side-groups attached to the edge of the molecule. These deviations from a prototypical PAH decrease the molecular stability, but at the same time are the origin of spectral variations needed to account for the totality of the AIBs. For instance, superhydrogenation and/or the presence of aliphatic side-groups (which include sp^3 hybridized carbon) can account for the 3.4 μm band (Mackie et al. 2018; Tielens 2008, and references therein).

Another range of structural variations that have been studied encompass the possibility of isomerization. This includes hydride shifts, which consist of one of the peripheral

hydrogens moving along the edge of the PAH (Trinquier et al. 2017a; Alvaro Galué & Oomens 2012). However, isomerization is not limited to hydrogen roaming and can also affect the carbon skeleton. In this sense a variety of routes have been explored, including dangling ethynyl/vinyl groups and the rearrangement of rings into hepta/septa/octagons (Bouwman et al. 2016; Trinquier et al. 2017b). For isomerization reactions to take place, an energy barrier specific for the rearrangement needs to be overcome. Isomerized PAHs also display different fragmentation pathways and bond dissociation energies can change with respect to regular PAHs.

The effects of the variations outlined here are studied using a combination of theoretical and experimental techniques. All of these lead to a better understanding of the driving mechanisms in PAH fragmentation and IR emission, but it is important to keep in mind that these techniques do not evolve independently. Experimental findings guide theoretical studies, which in turn provide predictions that need to be tested in laboratory settings. The main experimental and theoretical tools used for PAH research are described in more detail here.

1.5.1. Theoretical studies

Quantum chemical calculations have been invaluable when investigating the trends in stability and mid-IR emission associated with size and structural changes of PAHs. While experimental work is crucial in guiding and corroborating predictions from these calculations, they have technical limitations and time constrains which prevent the quick and efficient analysis of a large number of molecules. Laboratory work is limited by which molecules can be efficiently synthesized and carry a variety of instrumental effects, while quantum chemical calculations can tackle these issues on a large variety of molecular structures in a more time efficient manner. Nevertheless, theoretical calculations must be thoroughly corroborated against experiments to assess their range of validity. Among the theoretical tools available, density functional theory (DFT) is central to the work of this thesis and will be addressed in more detail. It must be noted, however, that this is by no means the only possible theoretical approach, which includes molecular dynamics and statistical methods as well.

The different energy levels within a molecule, whether electronic, vibrational or rotational, must be calculated using the Schrödinger equation. This relates the description of the kinetic and potential energy of the system to the energy values that are actually accessible. Unfortunately, none but the simplest of systems have analytic or even numerically exact solutions and thus, the use of approximations becomes imperative. In first place we have the Born-Oppenheimer approximation, which considers the nuclear motions independent from the electrons, as the former are much heavier than the latter. Using this it is possible to determine the equilibrium position for the nuclei and the electronic part of Schrödringer equation can then be solved independently. Here is where DFT comes into play, as the wavefunctions of individual electrons are replaced by an electron density, which is represented as a linear combination of functions which are part of the so called basis set. The electronic kinetic energy, together with the nuclei-electron and electron-electron interactions are then replaced by functionals of the electron density. Once this part of the equation has been solved, the nuclear po-

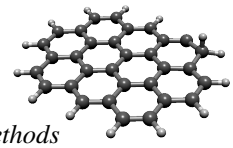

sitions have to be readjusted and the process continues iteratively until convergence. There are a number of basis sets and functionals available for these calculations and the particularities of the system under consideration must be taken into account when deciding which ones to use.

The immediate result of this type of DFT calculations is the energy of the molecule. In works regarding the fragmentation of PAHs, the different bond dissociation energies (BDEs) can be calculated following this method. In the case of direct H-loss, for instance, the energy of the final structure can be obtained using the same approach. The energy of the parent molecule can then be subtracted from this value, together with the energy of the lost hydrogen atom, yielding the BDE for this particular bond cleavage. The energy of other reactions, including isomerization and loss of more complex units, can also be calculated by finding the transition state(s) involved in the reaction. This requires finding a maximum in the potential energy surface that connect the products and reactants.

DFT calculations can also be carried one step further, allowing for the calculation of the vibrational modes of the molecule. After solving for the electronic portion of Schrödinger equation, attention can be shifted back to the nuclear interactions, with the interaction potential again requiring simplifying assumptions. While recently there has been great progress in the use of anharmonic potentials, for the most part the work has been limited to a quadratic, harmonic approximation (Mackie et al. 2015; Maltseva et al. 2015). The latter generally yields a good match with experimental data once a scaling factor is applied to the computed vibrational frequencies. In this thesis, all DFT calculations are limited to using the harmonic approximation, given that anharmonic calculations are much more computationally expensive and the gain in accuracy is not critical unless high resolution comparisons are needed.

The success of DFT calculations has resulted in multiple spectral databases (Malloci et al. 2007; Boersma et al. 2014), which in turn have guided the interpretation of astronomical mid-IR spectra. This has allowed for the classification and identification of shapes and intensities of mid-IR bands and plateaus as due to ionization, clustering and structurally different PAHs (e.g., Boersma et al. 2008; Rosenberg et al. 2014; Andrews et al. 2015).

1.5.2. Laboratory studies

Even with all the advances in quantum chemical calculations, experimental work remains crucial in testing the validity of theoretical studies and in guiding them. A wide range of experimental techniques are used to characterize different aspects of PAHs including, but not limited to, their spectra, reactivity and dissociation pathways. As usual, all of these have strengths and limitations, and it is through their combined use — with support from theory and models — that a full picture of the evolution of PAHs in space and their emission characteristics can be fully addressed.

Laboratory studies focus on (photo-)chemical reactions, exploring the dissociation channels and reactivity. The fragmentation pattern of PAHs upon irradiation has been well studied and found to always follow an overall similar pattern. The dehydrogenation shows enhanced intensity on even mass peaks with respect to odd ones (e.g., Ekern

et al. 1998; Zhen et al. 2014). Whether this is due to molecular hydrogen release or a sequential loss with low barriers for odd losses has been explored as well in the case of small PAHs ($N_C \leq 24$). While the H_2-loss pathway has indeed been detected it has generally been regarded as a minor channel with respect to sequential losses (Ling et al. 1995; Jochims et al. 1994). The process of superhydrogenation by interaction with carbon atoms has also been the subject of considerable studies, particularly as a potential pathway for H_2 formation (Thrower et al. 2012; Cazaux et al. 2016).

1.6. Experimental set-up

Experiments carried out as part of this thesis were performed with an in-house experimental set-up dubbed the "instrument for photodynamics of PAHs" (i-PoP; Zhen et al. 2014), which at its core consists of a commercially available quadrupole ion trap (QIT; Jordan C-1251) coupled to a time-of-flight mass spectrometer (TOF-MS; Jordan D-850). A diagram of the experimental set-up is shown in Fig. 1.11. These two units are located in separate high vacuum chambers, which are referred to as the source chamber and the detection chamber, respectively. Within the source chamber, the PAH/fullerene sample of interest is evaporated from an oven (Heat Wave Labs) by adjusting the temperature to that where the molecule under consideration begins to gently sublimate. The oven temperature is monitored using a thermocouple and the power supply allows for a maximum working temperature temperature of ∼700 K, enough for the evaporation of species with up to 70–80 C-atoms. Once the molecules are brought into the gas phase, they are ionized via electron impact from an electron gun (e-gun; Jordan C-950) and guided into the QIT with an ion gate. This consists of two plates at different potentials to lead the newly formed ions and a split Einzel lens to control the direction of entrance into the QIT. A DC voltage pulser (D-1040) controls the closing and opening of the ion gate, by switching the voltage in one of the half-plates of the Einzel lens that will redirect any additional ion away from the QIT. The working pressures of the source and detection chambers are $\sim 10^{-7}$ and $\sim 10^{-8}$ mbar, respectively.

1.6.1. Quadrupole ion-trap

The QIT consists of two hyperbolic metal electrodes at each end of the trap and a ring electrode set in the middle (Stafford et al. 1984). An AC voltage is applied to the ring electrode that allows for the ions to be trapped in the center, while their position oscillates in between the two end-cap electrodes. Given that no DC offset voltage is added, the stability of molecules within the ion trap is only determined by,

$$q_z = \frac{8eV}{m(r_0^2 + 2z_0^2)\Omega^2}, \tag{1.1}$$

where r_0 and z_0 are the dimensions of the trap, V and Ω are the amplitude and frequency of the AC voltage, respectively, and e and m are the charge and mass of the ion in question (for further details, see March 1997). Only molecules for which $q_z < 0.908$

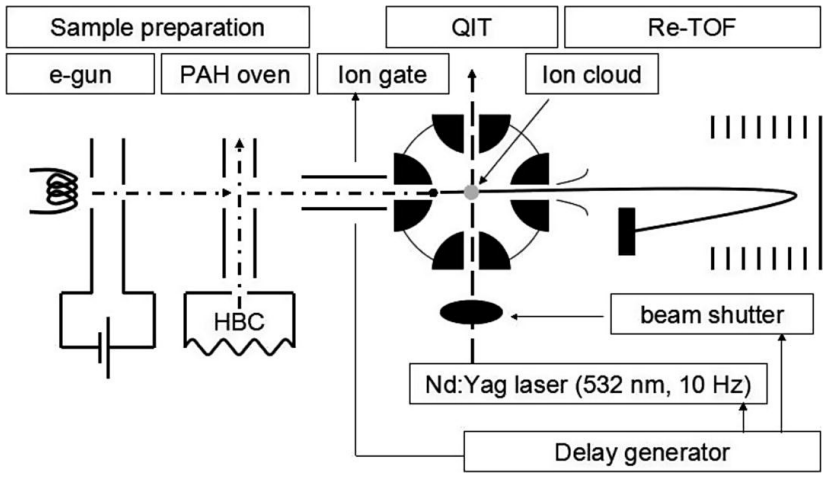

Figure 1.11.: Schematics of the instrument for photodynamics of PAHs (i-PoP). This diagram shows hexabenzocoronene (HBC) as the PAH sample. The sections of sample preparation and the QIT are part of the source chamber while the Re-TOF is part of the analysis chamber. The beam shutter and laser are situated out of vacuum. The operation cycle is controlled with a delay generator (Figure taken from Zhen et al. 2014).

fall inside the stability region of the QIT — i.e., ions below a certain mass-to-charge ratio are not trapped, with the specific cut-off given by the voltage amplitude used.

In order to remove excess kinetic energy from the PAH ions and thus increase the trapping efficiency, helium gas is leaked directly into the QIT. The pressure of this buffer gas results in an increased density of PAH ions within the QIT with respect to the background of the source chamber. By taking into account the pumping efficiency, it can be estimated that the pressure at the center of the QIT is 10^{-6}–10^{-5} mbar (Zhen et al. 2014). Through collisions with the injected helium gas, the highly excited PAHs will quickly thermalize at about room temperature — the temperature of the gas reservoir. This in turn reduces the size of the ion cloud to ∼1 mm (relevant for the overlap with the laser beam), concentrating the ions closely at the center of the QIT, increasing the trapping efficiency and helping as well in terms of the mass resolution.

Once the PAH ions have been trapped, they can be stored for a variable amount of time, during which mass isolation (described below) and/or irradiation can be set to occur. The irradiation can be conducted with the use of an Nd:YAG laser (DCR-3, Spectra-Physics) pumped dye laser (LiopStar-E with LSEH), or directly using only the former. In both cases doubling or tripling of the fundamental frequency can be applied and, by changing the particular dye, a wide range of wavelengths can be produced. Depending on the photon energy, the output of the laser will range from a maximum of ∼120 mJ at 532 nm (using the second harmonic of the Nd:YAG laser) to ∼10 mJ at 656 nm (the fundamental of the dye laser using DCM as a dye). The repetition rate of the laser system is 10 Hz, and the total number of pulses per experimental data point is controlled by an electromechanical shutter (Thorlabs SC05), located outside

the source chamber. Finally, the fragments generated are extracted from the QIT into the TOF-MS. This is achieved by applying a pulsed voltage from ground to +800 V onto one end cap electrode and from ground to −800 V onto the other, thus emptying the QIT and leading the ions into the detection chamber through a 2 mm skimmer.

1.6.2. MASS ISOLATION

As a side effect of the electron impact ionization from the e-gun, partial fragmentation of the precursor PAH may occur. This is mostly limited to a few hydrogen losses, but it can introduce difficulties when trying to separate the effect of photodissociation and electron induced fragmentation. Furthermore, even a relatively small PAH will inevitably show significant peaks corresponding to naturally occurring isotopomers. Throughout this thesis we only deal with pure hydrogen-carbon containing PAHs, which simplifies the number of possible isotopes that need to be dealt with. While deuterium is a stable hydrogen isotope, its natural abundance is too low to pose any significant contribution to the high mass peaks observed. On the other hand, ^{13}C has a natural abundance of ∼1.1%, making its contribution significant for the analysis of medium to large sized PAHs. For instance, coronene has a first isotopic peak with an intensity ∼25% of the pure $^{12}C_{24}H_{12}$. Even the second isotopic peak (corresponding to $^{13}C_2\,^{12}C_{22}H_{12}$) has an intensity of ∼6% and the isotopic fractions only increase with the number of carbons in the molecule.

The presence of secondary peaks at the beginning of the experiment complicate the analysis. In order to ameliorate this issue, a stored waveform inverse Fourier transform (SWIFT) pulse is used to refine the mass selection (Doroshenko & Cotter 1996). It consists on a time-domain waveform, created by calculating the inverse Fourier transform of the excitation spectrum. This includes the range of resonant frequencies which corresponds to the ions to be expelled from the QIT prior to irradiation. The SWIFT pulse is fed into one of the end-cap electrodes, thus exciting the molecules whose secular frequencies inside the trap correspond to those included in the excitation spectrum.

The capacity for single peak isolation is dependent on the mass of interest and the closeness of the peaks to be eliminated. As the molecular mass increases, the secular frequencies of successive masses are found closer together, thus making it harder to properly isolate a single mass. This is indeed limited by the resolution in the frequency-domain function, which in the present case limits the single peak isolation to molecules with $N_C \lesssim 30$. However, broad isolation can be performed even for high mass species, which results in about three different masses to be retained in the trap (e.g., the parent molecule, the first isotopomer and the monodehydrogenated parent molecule). If these are mostly limited to isotopic peaks, as shown in Fig. 1.12, then their contribution to the mass spectrum can be dealt with separately during the analysis. Since all isotopic peaks for PAHs have masses higher than that of the pure ^{12}C molecule, the lower mass peak in the spectrum can be considered isotopically pure. By knowing as well the number of carbon atoms within the molecule and the natural abundance of ^{13}C, the contribution of isotopically substituted forms of this peak can be removed from the following ones.

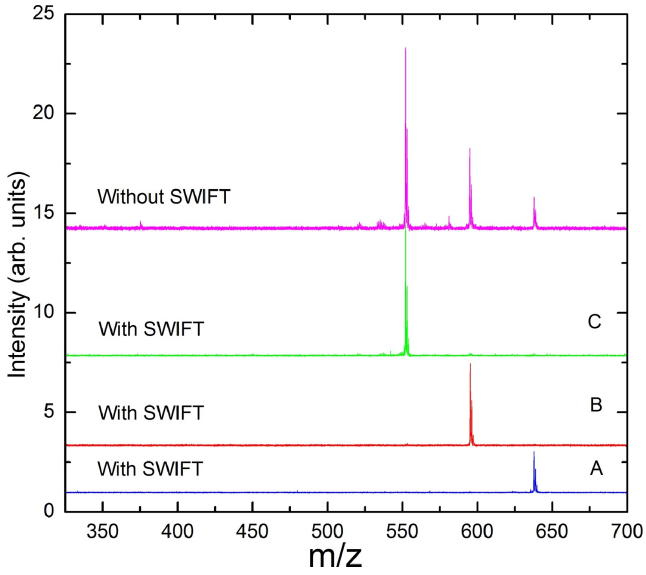

Figure 1.12.: Different SWIFT settings in the isolation of the main peaks of methyl- and methoxy-substituted hexabenzocoronene, recorded with i-PoP. Curve A corresponds to isolation of the parent molecule $(CH_3)_4(OCH_3)_2C_{42}H_{12}{}^+$, while curves B and C isolate the electron impact products after the loss of one and two OCH_3 units, respectively. Note that the mass spectrum without SWIFT shows only fragmentation induced by the e-gun (Figure taken from Zhen et al. 2016).

This is achieved using,

$$I'_j(I_i) = \binom{N_C}{j-i} p^{j-i} I_i, \tag{1.2}$$

where the term in brackets correspond to the binomial coefficient with j corresponding to the mass whose contribution of isotopomers from the peak with mass i is going to be removed from. I'_j is the intensity to be subtracted from peak j as a result of contributions from peak i (with $j > i$), p is the natural abundance of ^{13}C and I_i is the intensity of the isotopically pure peak i. Equation 1.2 assumes that the number of carbon atoms is the same between peak i and j, which is normally the case. After contributions from mass i are removed from higher mass peaks (up to four, depending on the size of the molecule), the process is repeated from the now isotopically pure intensity with mass $i + 1$.

1.6.3. Time-of-flight mass spectrometry

Once the ion of interest has been isolated and irradiated, the fragmentation products are transported into the detection chamber for their analysis. Before entering the TOF-MS, the ions are exposed to an electric field $\Phi(r)$, where r is the position within the ion trap, and then are left to evolve in the field-free tube. As individual ions are accelerated

into the TOF-MS, the initial energy can be considered to be only potential in the form $e\Phi(r)$, where e is the charge of the ion in question. Since the flight tube is field-free, the energy will be all converted into kinetic by the time it reaches the detector, leading to

$$e\Phi(r) = \frac{mv^2}{2}. \tag{1.3}$$

By taking the flight length d, we have $v = d/t$, where t is the time of flight of the particular ion. This gives us a relationship between the mass-to-charge ratio and the time of flight, namely,

$$\frac{m}{e} = \frac{2\Phi(r)t^2}{d^2}. \tag{1.4}$$

Typically the mass-to-charge ratio is given in terms of m/z in atomic units and the conversion between time and mass is given by a simple quadratic relationship.

The previous treatment is strictly valid for the case of a linear TOF-MS. In i-PoP, the detection chamber consists of a reflectron mass spectrometer. While the principle of operation is the same as before, an intermediate step where the ions are reflected into the detector is added. This results in an increased mass resolution, as more energetic ions will penetrate deeper into the reflectron potential, thus allowing for less energetic ions of the same mass to "catch up" with them. In this way, the effect of variations in the initial kinetic energy can be accounted for. For more information on the functioning of a reflectron, and TOF-MS in general, see Mamyrin (2001).

The detector itself is made of a multi-channel plate (MCP; Jordan C-701), which functions as an amplifier for ion signal. Under normal circumstances, the effect of a single particle is undetectable, but the high electric field of the MCP allows for individual particles hitting the channels to produce an electron cascade. The total signal gain has been estimated to be 2×10^8 (Zhen et al. 2014).

The recorded spectrum can then be analyzed in terms of the intensity of the detected peaks. Individual peaks have been fitted to a model function rather than integrated numerically, given that the former method allows for estimating the error in individual measurements. While fitting a Gaussian function to each mass peak provides a good zero-th order approximation, it does not take into account the asymmetry and non-standard kurtosis ("spikiness") of the actual data. To obtain a more proper fit and reduce the residuals, a Pearson IV distribution has been used for all the experimental data analysis (Pearson 1895). This function can be expressed as,

$$f(x) = Ak\left(1 + \left(\frac{x-\lambda}{\alpha}\right)^2\right)^{-m} \exp\left(-\nu \arctan\left(\frac{x-\lambda}{\alpha}\right)\right), \tag{1.5}$$

where the parameter A is related to the peak intensity and parameters λ, α, ν and m relate to the mean ($\mu \doteq \langle x \rangle$) and the moments ($\mu_i \doteq \langle (x-\mu)^i \rangle$, with i referring to the ith moment) of the distribution. In terms of the variance ($\sigma \doteq \sqrt{\mu_2}$), skewness

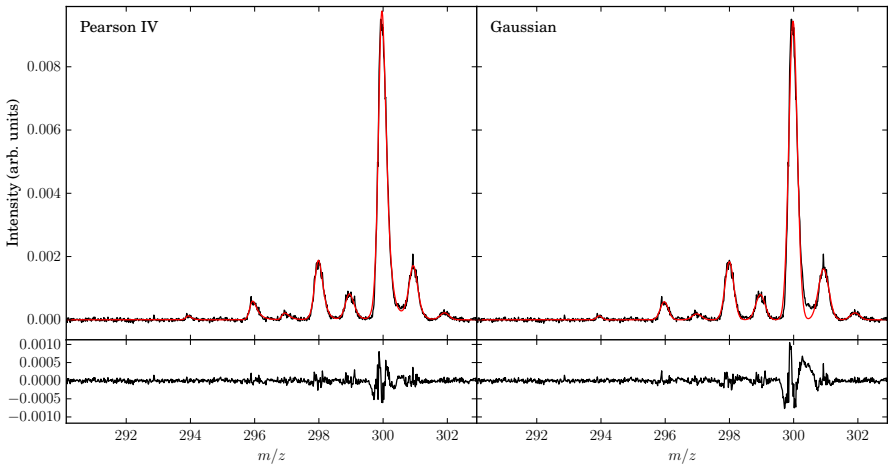

Figure 1.13.: Comparison of Pearson IV (left) and Gaussian (right) fits to a mass spectrum of the coronene cation ($C_{24}H_{12}{}^{+}$). The fragmentation corresponds to electron impact effects and the lower panels show the residual to the corresponding fit. Low intensity peaks are generally fit equally well, but a significant improvement can be observed for the fit of high intensity peaks, for which the wings are better accounted for.

($\gamma_1 \doteq \mu_3/\sigma^3$) and kurtosis ($\gamma_2 \doteq \mu_4/\sigma^4$), the relationships are given by,

$$\mu = \lambda - \frac{\alpha\nu}{r}, \tag{1.6}$$

$$\sigma = \sqrt{\frac{\alpha^2}{r^2(r-1)}}\sqrt{(r^2+\nu^2)}, \tag{1.7}$$

$$\gamma_1 = \frac{-4\nu}{r-2}\sqrt{\frac{r-1}{r^2+\nu^2}}, \tag{1.8}$$

$$\gamma_2 = \frac{3(r-1)\left[(r+6)(r^2+\nu^2)-8r^2\right]}{(r-2)(r-3)(r^2+\nu^2)}, \tag{1.9}$$

where $r = 2(m-1)$. In order for σ to be well defined, a constrain in the form $m > 1.5$ is placed on the fit. The parameter k in eqn. 1.5 is the normalization factor of the Pearson IV distribution, given by,

$$k = \frac{\left|\frac{\Gamma(m+i\nu/2)}{\Gamma(m)}\right|}{\alpha \mathrm{B}(m-0.5,\,0.5)}, \tag{1.10}$$

with Γ and B being the Gamma and Beta functions, which are defined as follows,

$$\Gamma(z) = \int_0^\infty x^{z-1}e^{-x}\,\mathrm{d}x, \tag{1.11}$$

$$\mathrm{B}(x,y) = \frac{\Gamma(x)\Gamma(y)}{\Gamma(x+y)}. \tag{1.12}$$

Given that the integral for $\Gamma(z)$ only converges if the real part of z is positive, it is required that $m > 0.5$, but this is less restrictive than the constrain on m set for the width to be well defined. A sample fit and comparison to an equivalent Gaussian fit is shown in Fig. 1.13.

1.7. THESIS CONTENTS

One key question in astronomy is to understand the organic inventory of space, particularly in regions of star and planet formation. Observations reveal that PAHs are an important component of the ISM and are key to the molecular universe. In particular, they may contribute to the formation of fullerenes as well as H_2 formation. This thesis focuses on the most stable products of PAH top-down chemistry and their relevance for astronomy in particular.

Chapter II is an exploration on the abundance and formation of C_{60} in PDRs. It includes a small scale survey searching for evidence on the universality of the anticorrelation between the intensity of the C_{60} and PAH bands. This is focused on a series of well studied PDRs encompassing a wide range of G_0 and density. The analysis is not limited to the mid-IR band intensity, but also compares the physical conditions of the PDRs to the PAH dehydrogenation model of Montillaud et al. (2013). This allowed to establish that, in the PDRs studied, both the level of PAH fragmentation and the observed band strengths are consistent with C_{60} formation through the fragmentation of PAHs.

In chapter III laboratory evidence is presented for the formation of fullerenes via photodissociation of large PAHs. The dissociation pattern of both fullerenes and PAHs shows the same enhanced peaks of pure carbon clusters, coinciding with the so called "magic numbers" of the fullerene family, which represent particularly stable structures. The decrease in C_{60} cross-section at 532 nm provides additional support for this formation pathway, as large PAHs irradiated at this wavelength only show little dissociation after the peak corresponding to C_{60} has been formed. Additional experiments are included, which suggest that the same conclusions could be drawn for the formation of C_{70}, thus connecting PAHs with the whole fullerene family and not exclusively C_{60}.

Chapter IV is an extensive experimental and theoretical study on the dehydrogenation of nine medium and large sized PAHs. The competition between sequential hydrogen loss and the formation of H_2 is explored in detail. Results from DFT calculations are put together into a detailed Monte-Carlo model that accounts for the effects of hydrogen roaming along the edge of the molecule, using experiments to guide the Monte-Carlo model. In concordance with other works, small PAHs are found to dehydrogenate sequentially, with exceptions for those that have a high proportion of trio hydrogens and bay regions. However, large PAHs show evidence for molecular hydrogen formation dominating the dehydrogenation process, at the very least in the first few steps. A divergence between DFT calculations with isomerization involving solo hydrogens and the experimental results is found, although the exact origin of this remains unclear. Most importantly, this work points toward H_2 formation from PAHs as a possibly efficient formation mechanism in PDRs.

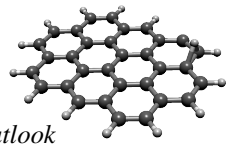

Finally, in chapter V, the previous results are applied to physical conditions typical of dense PDRs. As mentioned in Sect. 1.3.1, there is a known mismatch between the observed rate coefficient of H_2 production and the rates of established formation mechanisms. Here, molecular hydrogen formation as an outcome of PAH dissociation is investigated as a possible pathway to bridge this gap. Under ideal conditions, H_2 formation is found to be nearly two orders of magnitude larger than previously established, although it cannot account for the full mismatch. This work also reaffirms that H_2 formation through PAHs photodissociation dominates over abstraction from superhydrogenated PAHs. The latter process would only be effective deep inside molecular clouds and not at PDR photodissociation fronts.

1.8. Outlook

Within a few years, the launch of *JWST* promises to revolutionize the study of the AIBs. On the one hand, the increased sensitivity with respect to previous IR telescopes could allow for the detection of weak bands associated with PAHs, revealing more details of their general structure and hydrogenation state. While it is highly unlikely that a specific identification will take place, questions associated with heteroatom substitutions, the presence of aliphatic side groups and other "decorated" forms seems to be within reach. On the other hand, the increased angular resolution ($\sim 0\farcs2$) in spectral mapping will show the evolution of the mid-IR bands as the environmental physical conditions change, both in terms of the density and the UV field strength. For the first time, band shape and intensity shifts within single sources will be able to include the full range of the AIBs. Not only this, but the ability to map intensity variations at such resolutions will allow for comparisons with ALMA observations in order to search for small molecules thought to be by-products of PAH photodissociation and find correlations with AIB emission.

This thesis, together with other recent studies (e.g., Alvaro Galué 2014; Bouwman et al. 2016; Trinquier et al. 2017a,b), point to the importance of isomerization reactions for interstellar PAHs. Not only does this affect the photodissociation process, as demonstrated in this work, but also their IR signatures. Isomerized and partially fragmented PAHs are generally unavailable commercially, making it hard for their mid-IR spectra to be measured experimentally. Furthermore, the sheer number of possible isomers each PAH can have at varying degrees of fragmentation, would make even a purely theoretical treatment a titanic undertaking. However, the combination of QIT/TOF-MS techniques with infrared multiphoton dissociation (IRMPD; e.g., Oomens et al. 2001, 2006) spectroscopy can help in elucidating these questions. While IRMPD has drawbacks, particularly relating to relative band intensities, it can guide DFT calculations in identifying the structure of fragmentation products. The QIT/TOF-MS, coupled with isolation techniques such as SWIFT, allow for the selection of individual products, which can be probed using IRMPD.

The enhanced capacity of *JWST* with respect to its predecessors, poses a challenge to experimental and theoretical astrochemistry. Even considering the current understanding of the AIBs, a plethora of issues remain open on the molecular characteris-

tics of the emitters (the extent of nitrogen substitution, the degree of processing, etc.) and even on their emission process, particularly on the topic of anharmonic effects. The availability of *JWST* could certainly hold the key to answering these questions, it could also magnify the known problems with the PAH hypothesis. While the latter option seems problematic, it is also exciting, as it would open up the research scope on astronomically relevant, polyaromatic molecules. Continued experimental and theoretical studies, not only on classic PAHs, but on more exotic forms, still based on their basic structure, are absolutely critical in understanding the characteristics of the these complex organic molecules. Both approaches have their own inherent strengths and pitfalls, but in tandem — and guided by astronomical observations —, they can lead to accurate models of the interstellar PAH population, their evolution and the products of their photodissociation that could lead to further chemical complexity by merging top-down and bottom-up chemistry.